HHS Public Access

Author manuscript

Acta Biomater. Author manuscript; available in PMC 2016 December 01.

Published in final edited form as:

Acta Biomater. 2015 December ; 28: 76–85. doi:10.1016/j.actbio.2015.09.031.

Surface Chemistry Regulates Valvular Interstitial Cell Differentiation In Vitro

Matthew N. Rush[1,2], **Kent E. Coombs**[1,3], and **Elizabeth L. Hedberg-Dirk**[1,2,4,*]

[1]Center for Biomedical Engineering, University of New Mexico, Albuquerque, NM, USA

[2]Nanoscience and Microsystems Engineering, University of New Mexico, Albuquerque, NM, USA

[3]Biomedical Science Graduate Program, University of New Mexico, Albuquerque, NM, USA

[4]Chemical and Biological Engineering, University of New Mexico, Albuquerque, NM, USA

Abstract

The primary driver for valvular calcification is the differentiation of valvular interstitial cells (VICs) into a diseased phenotype. However, the factors leading to the onset of osteoblastic-like VICs (obVICs) and resulting calcification are not fully understood. This study isolates the effect of substrate surface chemistry on *in vitro* VIC differentiation and calcified tissue formation. Using ω-functionalized alkanethiol self-assembled monolayers (SAMs) on gold [CH_3 (hydrophobic), OH (hydrophilic), COOH (COO^-, negative at physiological pH), and NH_2 (NH_3^+, positive at physiological pH)], we have demonstrated that surface chemistry modulates VIC phenotype and calcified tissue deposition independent of osteoblastic-inducing media additives. Over seven days VICs exhibited surface-dependent differences in cell proliferation (COO^- = NH_3^+> OH > CH_3), morphology, and osteoblastic potential. Both $NH_3^+$and CH_3-terminated SAMs promoted calcified tissue formation while COO^--terminated SAMs showed no calcification. VICs on NH_3^+-SAMs exhibited the most osteoblastic phenotypic markers through robust nodule formation, up-regulated osteocalcin and α-smooth muscle actin expression, and adoption of a round/rhomboid morphology indicative of osteoblastic differentiation. With the slowest proliferation, VICs on CH_3-SAMs promoted calcified aggregate formation through cell detachment and increased cell death indicative of dystrophic calcification. Furthermore, induction of calcified tissue deposition on NH_3^+ and CH_3-SAMs was distinctly different than that of media induced osteoblastic VICs. These results demonstrate that substrate surface chemistry alters VIC behavior and plays an important role in calcified tissue formation. In addition, we have identified two novel methods of calcified VIC induction *in vitro*. Further study of these environments may yield new models for *in vitro* testing of therapeutics for calcified valve stenosis, although additional studies need to be conducted to correlate results to *in vivo* models.

Corresponding Author: Elizabeth L. Hedberg-Dirk, Address: Center for Biomedical Engineering, MSC01 1141, 1 University of New Mexico, Albuquerque, NM 87131, edirk@unm.edu, Fax: 505-277-6209, Phone: 505-277-5906.
Alternate Author Email:
Matthew N. Rush, mrush@unm.edu
Kent E. Coombs, kcoombs@salud.unm.edu

1. Introduction

Valvular heart disease (VHD) is estimated to affect 2.5% of the US population with a disproportionate impact on an increasing elderly community.[1, 2] Derived from infections, valve degeneration, or genetic disorders, VHD can manifest as regurgitation or stenosis of the valve. As a result of obstructed blood flow, valve stenosis generates transvavlular gradients that triggers compensatory ventricular hypertension, leading to increased risk for other cardiovascular disorders.[1–3] As such, VHD represents a significant health risk worldwide. Furthermore, there will continue to be rises in the prevalence of VHD as the elderly population grows due to advances in medical technology.[1–5]

The leading cause of VHD is valve stenosis, which is characterized by valve thickening, increased protein deposition, and eventual calcification.[3, 4, 6] The primary driver for valvular calcification is the differentiation of valvular interstitial cells (VICs) into a disease inducing phenotype.[6, 7] However, the factors leading to the onset of VIC differentiation and resulting calcification are not fully understood and a more complete characterization of VIC differentiation and phenotypic change is required before treatment of valve disease can be realized.

As the predominant cell type within the valve, VICs are responsible for valve formation, remodeling, and tissue homeostasis. VICs are a heterogeneous population that undergo phenotypic change regulated by environmental factors. VICs have been shown to alter phenotype in response to soluble factors,[8–11] substrate stiffness,[6, 8, 12–15] and surrounding extracellular matrix proteins.[8, 10, 11, 16–21] Although phenotypic change is a dynamic event, literature tends to compartmentalize VIC function in order to clarify and separate the underlying causes.[22]

VICs are commonly characterized by their quiescent (qVIC), activated (aVIC), and disease phenotypes. In a normal adult valve, qVICs are thought to preserve physiological structure and function while maintaining a low level of matrix synthesis and degradation inhibiting angiogenesis.[22] Following injury or abnormal hemodynamic/mechanical stress, VICs become activated (aVICs, myofibroblastic) and are associated with increased extracellular matrix secretion and expression of various biological markers including α-smooth muscle actin (α-SMA), matrix metalloproteinases, and transforming growth factor-β.[22, 23] Activated VICs exhibit increased contraction, prominent stress fiber formation, increased proliferation, and migration.[22] *In vitro*, aVICs display an elongated morphology and form orthogonal patterns of overgrowth resembling hills and valleys.[6] Upon completion of remodeling or wound healing, most aVICs are eliminated by apoptosis or reversion to qVICs.[24]

When VIC dysregulation or abnormal extracellular matrix production occurs, conversion to diseased phenotypes results in pathological fibrosis and calcification of the valve.[10, 24] The mechanisms of VICs tissue calcification have been intensely study and currently two processes have been proposed. [5, 25–27] Dystrophic calcification is a passive degenerative process characterized by early cell injury and deposition of calcium associated with tissue

damage and necrotic cells. [10, 25, 26] Alternatively, osteogenic calcification (ossification) is an active process involving bone and cartilage development, marked by the expression of various osteogenic markers. [7, 25, 26, 28] *In vitro*, VICs undergoing osteogenesis, osteoblastic-like VICs (obVICs), are characterized by a round/rhomboid morphology followed by the formation of three-dimensional calcified nodules. It is important to note, that these two processes are not mutually exclusive as a common activator of tissue calcification, TGF-β, has been shown to lead to cellular apoptosis as well as nodule formation.[10] However, different processes may arise due to variations in signaling in the cellular microenvironment. Forced obVIC differentiation *in vitro* is commonly achieved by adding soluble signaling factors (β-glycerophosphate, ascorbic acid, and dexamethasone) to media. However, spontaneous *in vitro* nodule formation in media lacking osteoblastic inducing additives,[8] as well as calcification of decellularized biological valves *in vivo*, suggests calcification may be mediated by additional physical cues.[29]

To understand how surface chemistry correlates to VIC behavior and initiation of valvular disease, we used alkanethiol self-assembled monolayers (SAMs) of ω-functionalized alkanethiolates on gold as model substrates with uniform chemistry. The chemisorption of thiols to gold and the hydrophobic interactions of alkane chains results in stable, ordered, and well-packed monolayers (Figure 1).[30] As such, SAMs offer well-defined models for systematically investigating phenotypic change directed by surface chemistry. Four physiologically relevant functional groups were used to assess the effects of substrate hydrophobicity and charge on VIC phenotypic behavior. Due to the negatively charged environment present during valvulogenesis through increased hyaluronic acid expression, it was hypothesized that anionic functional groups would result in VIC activation and tissue production.[31, 32]

2. Materials and Methods

2.1. Reagents and Chemicals

All chemicals were purchased from Sigma-Aldrich chemicals unless otherwise noted. All cell culture media and reagents were purchased from Thermo Fisher Scientific, unless otherwise noted.

2.2. Fabrication of Self Assembled Monolayers

Gold-coated round 15 mm glass cover slips (26021, Ted Pella Inc.) were used as substrates for self-assembled monolayer (SAMs) formation. Coverslips were etched for 30 minutes prior to gold deposition in Piranha solution [70% (v/v) concentrated H_2SO_4, 30% industrial grade H_2O_2 (KMG Chemicals)] rinsed with diH_2O, and blown dry with N_2. Gold coating was conducted by sequential electro-evaporation of optically transparent films of chromium, adhesion layer (2 nm; High Vacuum Evaporator Systems), followed by gold (30 nm, 99.99% purity; Plasmaterials). Metal deposition was accomplished at 2 nm/s using a Thermionics VE-90 vacuum Evaporation System (TLI Enterprises) with chamber pressures at or below 1×10^{-5} Torr. Freshly prepared gold substrates were immersed in 1mM ethanolic alkanethiol solutions [1-dodecanthiol (47-136-4); 11-mercapto-1-undecanol (447528-16); 11-mercaptoundecanioc acid (450561-5G); 11-amino-1-undecanethiol,

hydrochloride 1N NaOH (A423, Dojindo Laboratories)] and SAMs were allowed to assemble for 12 hours.[30, 33] Etched cover glass and gold-coated controls were incubated alongside SAMs in absolute ethanol. Before use or characterization, samples were cleaned of unbound thiols in absolute ethanol and dried with N_2. In order to obtain desired charge on COOH (COO^-) and NH_2 (NH_3^+) surfaces, samples were rinsed in 1N basic (NaOH; EMD) and acidic (HCl; EMD) ethanol solutions, respective of charge group, blown dry with N_2 and then cleaned.[34]

2.3. Contact Angle Measurements

Static contact angles and images were evaluated using the sessile drop technique on a Model 100-00-115 Advanced goniometer (ramé-hart Inc.). Briefly, 5 μL of ultrapure water was pipetted onto sample surface and the contact angles were measured immediately after drop formation to minimize the effect of dynamic surface wetting and evaporation. Contact angle measurements between the water droplet and the sample surface were determined using DROPimage Standard software (ramé-hart).

2.4. X-Ray Photoelectron Spectroscopy (XPS)

XPS survey and high resolution spectra were obtained using Axis Ultra spectrometer (Kratos Analytical Ltd.) with a monochromatic Al K(α) (1486.6 eV) source at 225W. High-resolution spectra of carbon and oxygen were obtained for three areas for each sample at 30° and 90° take-off angles. Electron pass energy of 20 eV was used to analyze the regions of interest and curve fitting was performed on each spectral region to calculate atomic percentages. Base pressure was less than 5×10^{-9} Torr. Charge compensation was accomplished using low energy electrons. Linear background was used for elemental quantification of C1s and O1s spectra. Quantification utilized sensitivity factors provided by the manufacturer. All the spectra were charge referenced to Au at 84 eV. Curve fitting was carried out using individual peaks of constrained width, position, and 70% Gaussian/ 30% Lorentzian line shape.

2.5. Atomic Force Microscopy

Scanning was performed at 2.50 μm/s (0.25 Hz) using a super sharp silicon probe (SSS-NCH, r > 5nm, Nanoworld) on an MFP3D-BIO (Asylum Research).

2.6. Ellipsometry

Freshly prepared samples were analyzed for film thickness using a Nanofilms EP3 optical ellipsometer @ 532nm (Accurion). Samples were collected at an incident angle of 70° for three areas on three different samples. The layer thickness was calculated using an index of refraction n = 1.52.[35, 36]

2.7. Primary Cell Extraction & Characterization

VICs were obtained through primary cell extraction from recently excised pig hearts (Hormel Foods Corp.) shipped overnight on ice. Aortic heart valves leaflets were removed and washed in 25 mL Dulbecco's phosphate buffered solution (DPBS) containing 2% (v/v) penicillin/streptomycin (P/S, Life Technologies). Three hearts (9 leaflets) were combined in

25 mL collagenase solution [12,500 units collagenase (LS004174, Worthington Biochemical Grp.) in 50 mL Media 199 (Hyclone, SH30253.01)] filtered through 22 μm Steriflip unit (Millipore) and incubated at 37°C for 15 min with gentle agitation. Both sides of leaflets were scraped and rinsed in DPBS. Leaflets were then incubated with 25 mL fresh collagenase solution at 37°c for 60 min with gentle agitation. Leaflets were vortexed for 2 min to break free loosely attached cells. Supernatant was collected and filtered through 100 μm cell strainer (BD Falcon). To remove valvular endothelial cells (VECs), cell solutions were incubated with 50 μL of magnetic beads labeled with CD31 antibody (Dynabead CD31, Life Technologies) at 4°C for 30 minutes with occasional mixing. Dynabeads were removed by magnetic separation. VICs were then placed in a new conical tube and centrifuged. Supernatant was removed and cells were re-suspended in VIC media [Media 199 (Hyclone), 10% FBS, 1% P/S, & 1% Fungizone]. Cells were seeded in T75 flasks (collagenase sample), and remaining leaflet material was diced up and plated into 6-well plates (Corning), 1 leaflet/well, to allow remaining VICs to migrate from leaflet (explant sample).

VICs were incubated (37°C, 5% CO_2, ~90% RH) and grown for 7–10 days, with media changes every other day. Cell supernatant was removed from T75 flasks after 2 days of attachment. Heart valve leaflets were removed from well plates after 3 days. Cells were grown to 70% confluence and enzymatically detached from surface with 2 mL of .25% (w/v) trypsin (Life Technologies). Collagenase and explant samples were combined in M199 media with 10% FBS (v/v) and 10% DMSO (EMD), and cryogenically frozen until use. VICs were seeded on SAMs between passages 3–4.

2.8. Cell Growth & Viability

Before seeding on substrates, VICs were thawed and grown till 80% confluence, to ensure cell viability. For all experiments, substrates were equilibrated with complete growth media [Medium 199, 10% fetal bovine serum, 1% penicillin/streptomycin, 1% fungizone] prior to cell seeding at 21,500 cells/cm^2. Media was replaced after 12 hours to remove unbound cells (attachment) and changed every two days. Osteoblastic controls were grown in OB media [Media 199, 10% fetal bovine serum, 10mM β-glycerophosphate, 2 mM ascorbic acid, & 10^{-7}M dexamethasone] [6] after initial 12-hour attachment. Substrates were rinsed prior to testing. Cell attachment and proliferation was assessed after 12 hours, and at 3, 5, & 7 days using MTT calorimetric assay (30–1010K, ATCC) according to manufacturer's instructions.

VIC viability was further investigated using AlexaFluor 488 Annexin V/Dead cell apoptosis kit (V13241, Life Technologies) according to manufacturer's instructions. Briefly, at 12 hrs and 5 and 7 days, culture media was removed and retained for apoptotic/dead cell concentrations while attached cells were enzymatically removed from surfaces. Cells were centrifuged, supernatant removed, and cell pellet re-suspended in 1× annexin binding buffer. Necrotic controls were achieved by incubating with 70% (v/v) ethanol. Apoptotic controls were achieved by leaving cultures at room temperature overnight. All samples were incubated with 100 μL staining solution [5 μL Annexin V and 1 μL propidium iodide @ 100μg/mL in 1× annexin binding buffer] for 15 minutes. Samples were read on Accuri C6 flow cytometer (BD Bio.).

2.9. Calcium Content

After 5 and 7 days, calcium deposition was visualized by incubating cells with the anthriquinone dye alizarin red S (ARS), forming a complex via chelation. Briefly, culture medium was aspirated and cells were rinsed 3× with DPBS followed by fixation using 10% formalin for 1 hour. After fixation, 100 μl of 40 mM ARS staining solution (pH 4.1) was added to each well and incubated for a minimum of 30 minutes in the dark at room temperature. [6] Upon completion the ARS solution was aspirated and the wells were rinsed 3× with diH20 then PBS in order to ensure removal of non-specific ARS stain. Samples were imaged under brightfield with phase contrast 10× magnification objectives (Eclipse TS1000). Calcified tissue and nodule diameter was determined using Image J (NIH).

2.10. Gene Expression

All reagents for gene expression were purchased from Life Technologies unless otherwise noted. mRNA was extracted from cell samples using RNAeasy plus micro kit (Qiagen 74034) with gDNA removal, according to manufacturer's instructions. Total mRNA content was analyzed using Nanodrop UV/Vis Spectrometer (Model 2000c, Thermo Fisher Sci.) and reverse transcription carried out using GoScript reverse transcriptase system (Promega). Gene expression of αSMA/ACTA (Ss04245588_m1), osteocalcin/BGLAP (Ss03373655_s1), collagen I-α2 (Ss03375690_U1), and elastin (EMLIN: Custom Primer#AJLJIR9) were analyzed using TaqMan Gene Expression master mix, according to manufacturers specifications, and measured on a StepOne Real Time-PCR (Applied Bio). Data was collected and analyzed using StepOne software v2.2.2. All samples were compared to GAPDH (Ss03374854_g1) endogenous controls.

2.11. Immunocytochemical (ICC) Staining

Cells were fixed with 10% formalin for one hour and washed twice with DPBS. Cells were then permeabilized with 0.01% (v/v) Tween20 in DPBS (PSBT) for 15 min followed by reactive ion removal using 10% (m/v) sodium azide and 10μM H_2O_2 in PBST. Samples were incubated with primary antibodies (αSMA, ab7817) diluted 1:75 in a 3% (w/v) BSA solution for 90 minutes. Primary antibodies were removed and samples washed twice with PBST followed by secondary antibodies goat anti-mouse AlexaFluor 488 (A11001, Invitrogen) 1:400 in DPBS incubation for 90 minutes. Cells were counter stained with DAPI in DPBS (1:1000, Invitrogen) for 5 minutes. Samples were mounted (Fluoromount, F4680-25ML) on glass slides and sealed with clear nail polish. Samples were imaged on a Zeiss LSM 510 META microscope with 40× oil 1.3 NA objective.

2.12. Statistical Analysis

All results were analyzed using one-way analysis of variance followed by Tukey-Kramer post hoc analysis with Sidak correction for multiple comparisons and a 95% confidence interval ($p < 0.05$). All analyses were done using Prism 6 software (GraphPad).

3. Results

3.1. Surface Characterization of Self-Assembled Monolayers

Self-assembled monolayers expressing four different functional groups (CH_3, OH, COO^-, NH_3^+) were used as model surfaces to assess the effect of substrate chemistry on VIC phenotype. These four chemistries exhibit different degrees of wettability and charge. CH_3-SAMs are non-polar and relatively hydrophobic, whereas, OH, COO^-, and NH_3^+ are relatively hydrophilic. At physiological pH (7.4) partially ionized COOH and NH_2 SAMs present negative or positive charges, respectively (COO^- and NH_3^+).[34, 35] Gold-coated and uncoated glass were run as negative control substrates. Results from all experiments performed showed no statistical difference between the gold (Au) and glass controls. Therefore, only Au data will be included here. As current methods of osteoblastic differentiation utilize supplemented media, obVIC-media induced positive control samples on glass were used. All surface treatments and controls were characterized prior to VIC studies.

Static water contact angles of SAMs measured by goniometry are summarized in Figure 1. Measured values are in agreement with those reported in literature.[33, 37] X-ray photoelectron spectroscopy analysis of surface chemistry agrees with theoretical percentages (Supplemental Figure I). Ellipsometric measurements of SAMs indicate monolayer formation, with confirmation by atomic force microscopy (Supplemental Figure II and Table 1).[34, 35]

3.2. Proliferation and Cellular Density of VICs

Initial differences in the number of attached cells were observed within the first 12 hours (Supplemental Figure III). CH_3-SAMs resulted in significantly lower attachment (53% of attachment average) as compared to all other treatments when seeded at 21,500 cells/cm^2. Results reflect literature showing decreased cell adhesion to hydrophobic surfaces.[37–39] In order to provide uniform seeding density all subsequent experiments were seeded at 43,000 cells/cm^2 on CH_3-SAMs and 21,500 cells/cm^2 on all other surfaces ensuring no significant difference in initial cell density between treatments (Figure 2).

Proliferation of VICs was assessed over seven days, demonstrating variations in growth rate due to substrate chemistry. A lack of initial proliferation on CH_3 and OH-SAMs resulted in a significantly lower cell concentration at day 3. Over the same time, VICs on glass induced with OB media demonstrated the greatest proliferation rate and significantly higher cell concentration. All other treatments (Au, COO^-, and NH_3^+) resulted in a moderate initial proliferation (Figure 2). Differences in proliferation rate continued through 5 days (Figure 2). During this time, COO^--SAMs promoted the greatest proliferation rate. After 7 days in culture, however, all treatments except CH_3-SAMs resulted in VIC confluence inhibiting further proliferation (Figure 3).

3.3. Morphological Variation Between Surfaces

Upon attachment (12 hrs), VICs adopted a characteristic elongated morphology on all treatments with the exception of CH_3-SAMs, which exhibited cellular aggregates and areas

of increased cellular density with large cell-free regions (Figure 3). On CH_3, OH, and osteoblastic-induced samples a small subset of VICs maintained a spherical morphology but remained anchored after media changes (Figure 3).

By day 3 VICs on all surfaces exhibited an elongated morphology (Figure 3). However, between days 3 and 5, significant morphological differences amongst treatments emerged. Individual VICs in OB media adopted a round/rhomboid morphology and spread to fill the entire growth area. Similar round/rhomboid VIC morphology was exhibited by NH_3^+, CH_3, and OH-SAMs to varying degrees (Figure 3, Supplemental Figure IV–V). VICs on COO^--SAMs and Au maintained elongated morphology through 5 days.

By day 7 VICs on Au, OH, and COO^--SAMs adopted highly aligned cellular confluent cultures, generally exhibited by aVICs,[6, 22] while VICs in OB media and on NH_3^+-SAMs tended to adopt a round/rhomboid morphology with non-linear/spread confluent cultures (Figure 3). As the only surface not to reach confluence, VICs on CH_3-SAMs adopted a round morphology in lower density regions, and formed clustered aggregates in higher density areas. The tendency for cellular aggregates on CH_3-SAMs to partially detach from the surface led to the formation of sheeted aggregates semi-suspended in culture media (cell sheets). Cell sheets were typically bound by a single edge resulting in the cell sheet folding back upon itself (Supplemental Figure VI).

3.4. Development of Calcified Nodules

At confluence (day 7), cells on all treatments except COO^--SAMs and osteoblastic culture exhibited some degree of calcified tissue formation (Figures 3 and 4). On CH_3-SAMs early cellular clustering resulted in the formation of large cellular aggregates (221 ± 123 μm). On Au and OH-SAMs, small spherical nodules were observed infrequently and the nodules were typically small (30–60 μm), indicative of recent formation. Distinct from all other treatments, VICs grown on NH_3^+-SAMs exhibited nodule formation by day 5, which increased in size (115 ± 40 μm) and frequency by day 7 (Figure 3 and Table 1). VICs grown in OB media exhibited no nodule formation through 7 days, consistent with the observation that nodules typically appear between 14 and 21 days under supplemental media conditions (without TGF-β).[6, 8, 40] Small nodules were observed on OB cultures when cultured out to 14 days (Supplemental Figure VII).

Nodule formation is typically accompanied by apoptosis and deposition of Ca_{2+}. In order to determine calcium deposition and apoptosis/necrosis, samples were stained with alizarin red S and imaged using bright field microscopy, or evaluated by flow cytometry using annexin V and propidium iodide. After 7 days, VICs grown on COO^--SAMs were the only cells to lack nodule formation or calcium staining (Figure 4). On Au and OH-SAMs VICs exhibited few small alizarin red S stained nodules, while VICs on CH_3-SAMs exhibited calcium within cellular aggregates with no distinct boundary. OB media induced VICs exhibit some cellular alizarin red S staining, but no aggregate nodular structures were observed. NH_3^+-SAMs, however, developed tightly bound, spherical calcium nodules with significant alizarin red S staining (Figure 4, arrows). When apoptosis was assessed at day 7, VICs exhibited equivalent levels of apoptosis on all treatments (Figure 5a). Overall cell death,

staining positive for annexin V and propidium iodide, was statistically elevated on CH_3-SAMs (Figure 5b).

3.5. Genetic Analysis of Phenotypic Markers

In order to determine phenotypic expression of VICs, samples were tested for common genetic markers. The development of contractile α-SMA cytoskeletal filaments is an accepted indicator of activation.[22, 41] At 3 and 5 days VICs grown on NH_3^+-SAMs and OB media exhibited a significant up-regulation of α-SMA mRNA expression compared to other treatments (Figure 6A). Similar up-regulation was observed in VICs stained for α-SMA using immunocytochemical techniques (Supplemental Figure V). Osteocalcin (OCN), a late-stage marker of OB differentiation[6, 22] that typically accompanies the onset of nodule formation was tested at 5 and 7 days of culture. By day 7, VICs grown on NH_3^+-SAMs showed significant increase in OCN mRNA expression over all other treatments, including media induced obVICs (Figure 6B). In order to assess tissue production, collagen I and elastin mRNA expression were quantified at 3 and 5 days (Figure 7). After 3 days, collagen is up regulated on NH_3^+-SAMs and media induced osteoblastic controls. Elevated collagen expression was also observed on CH_3-SAMs, but results were not statistically different from Au controls. By day 5, all SAMs treatments are significantly lower than Au controls. Elastin expression is elevated on NH_3^+ surfaces at day 5, accompanying nodule formation.

4. Discussion

Many factors influencing VIC phenotype have been studied in the hope of understanding calcified nodule formation and controlling *in vitro* culture for healthy tissue production.[6, 8–11, 17–21] Previous research investigating the effect of distinct protein adlayers on VIC phenotype has attempted to control the cellular binding environment through adsorption and presentation of specific proteins onto tissue culture polystyrene.[6, 8–11, 17–21] However, the non-homogeneous surface of tissue culture substrates causes random deposition of proteins with uncontrolled orientations,[8, 42] resulting in conflicting results in literature.[18, 20]

4.1. Alkanetiolate Self-Assembled Monolayers

The uniform SAMs surface chemistry allows for controlled protein deposition and orientation, producing distinct and reproducible culture surfaces for understanding cell behavior in different microenvironments.[37, 38, 42, 43] In previous work, it has been observed that proteins in culture adsorb at a faster rate than cell attachment, and dictate cell-surface interactions.[38, 44] Specifically the adsorption of proteins to hydrophobic/hydrophilic and charged surfaces has shown that specific extracellular matrix proteins bind in a surface dependent manner, with variability in their tertiary structure, resulting in variation in available cellular attachment domains.[37–39, 43, 45]

4.2. Media-Induced Osteoblastic VICs

As a positive control VICs were grown in OB media on glass. Observed increases in proliferation rate and cell spreading resulting in confluent cell sheets is similar to results

reported in literature.[6] While calcification never occurred in OB media cultures within the seven days examined in this study, cultures were take out to 14 days to confirm nodule formation in our controls. Previous research indicates nodule formation occurs between 14–21 days in low-density (<25,000 cells/cm^2) cultures following the development of αSMA stress fibers, cellular detachment, and contraction.[6, 9, 40] For this reason αSMA is considered necessary for osteoblastic differentiation, suggesting that qVICs must go through activation to result in obVICs and tissue calcification.[9, 23] However, our results on CH_3-SAMs suggest a direct transition through well-defined stress fiber formation (quiescent → activated → osteoblastic) is not always necessary for the development of calcified tissues, similar to previous observations of dystrophic calcification caused by increased cell death.[10]

4.3. Non-activated VIC Calcium Deposition on CH_3-SAMs

As hydrophobic CH_3-SAMs have been shown to irreversibly adsorb and denature proteins resulting in loss of cellular binding domains, CH_3-SAMs provide a look into changes in VIC phenotype that result from low cell adhesion.[38, 39, 44] The slow proliferation, cellular aggregation, and formation of loosely adhered cell sheets suggest minimal interaction between the VICs and CH_3-SAMs. As such, the early aggregate behavior of VICs is likely the result of cell-cell adhesion to compensate for a lack of cell-surface adhesions.

Previous experiments have shown the release of mechanical tension on VICs also leads to increased apoptosis and ***in vitro*** calcification.[6, 7, 46, 47] Increased αSMA expression typically accompanies nodule formation, thus, calcification on hydrophobic surfaces without elevated αSMA expression suggests that VIC detachment may result in calcification without the need for αSMA-mediated contraction.[9, 23] Higher Ca^{2+} deposition under hydrophobic conditions are therefore likely related to the high cell necrosis levels observed through classical dystrophic mechanisms of cell death resulting in release of intracellular calcium and aggregation under this condition. Previous results by Jain B. ***et al.*** have shown that tissue calcification *in vitro* does not require cellular contraction and spherical nodule formation to induce apoptosis and calcium deposition.[6, 10] As such, inhibition of cell adhesion and possibly altered integrin and cell-cell signaling may explain the triggering event for increased cell death and Ca^{2+} deposition under these experimental conditions.[6, 48] Further studies are needed to determine if this observed behavior is exemplary of *in vivo* disease development.

4.4. Osteoblastic VIC Differentiation on NH_3^+-SAMs

With increased proliferation, elongated morphology, and increased αSMA expression over other functionalized SAMs, VICs grown on NH_3^+ surfaces exhibit early myofibroblastic behavior. With the onset of a round/rhomboid morphology, robust nodule formation, and OCN expression NH_3^+-SAMs undergo a clear transition from an aVIC to obVIC phenotype between days 3 and 5. The expression of OCN, a late stage osteoblastic marker, and the early appearance of calcified nodules suggests an accelerated transition between activated and osteoblastic phenotypes on cationic surfaces. Such behavior correlates with the observed osteoblastic differentiation of pre-osteoblastic cells on NH_3^+ surfaces.[39] Compared to the soluble factors used in OB media induction, the rapid obVICs differentiation on NH_3^+-

SAMs is controlled by cell-surface interactions, as no media additives are present. As no calcium deposition and gene expression in osteoblastic culture were observed during this same period, the accelerated obVIC behavior is likely the result of a novel signaling pathway in VICs induced by cell-material interactions specific to protein adsorption on NH_3^+ surfaces. NH_3^+-SAMs have been shown to preferentially adsorb greater amounts collagen and fibronectin than other hydrophilic groups (COO^- and OH).[43] However, currently literature on the influence of collagen and fibronectin on VIC nodule formation is conflicting.[10, 18–20] These differences may be due to differences in processing of the extracellular matrix proteins in these studies. Interestingly, NH_3^+-surfaces also resulted in a significant up-regulation of elastin expression over all other surfaces, which seems to correspond with development of nodules in culture at day 5. As fibronectin is required for microfibril formation onto which elastin is deposited, the early availability of fibronectin on NH_3^+-SAMs may be at least partially responsible for increased rate of nodule formation by VICs.[49, 50]

4.5. Delayed Growth on OH-SAMs

Previous research has demonstrated decreased protein adhesion on OH-SAMs, and thus, lower levels of binding domains available for cell attachment and proliferation.[36, 37, 45, 51] In this study VICs have shown limited attachment and proliferation over the first 3 days, but do not undergo significant apoptosis (Figure 5). No significant increase in collagen or elastin mRNA expression was observed up to 3 days in culture. However, collagen expression increased through 5 days. The increased cell spreading and proliferation of VICs on OH-SAMs suggests secretion of ECM proteins by VICs on these surfaces is sufficient to maintain viability and recover cellular functions. Lack of OCN expression and adoption of an elongated morphology forming highly aligned cultures suggests OH-SAMs serve to maintain the aVIC phenotype. However, as VICs on OH-SAMs eventually lead to nodule formation at high cell densities, OH substrates may not be ideal for VIC expansion *in vitro*.

4.6. Non-Osteoblastic Activation of VICs on COO^--SAMs

The activation of VICs on COO^--SAMs characterized by rapid proliferation and maintenance of an elongated, myofibroblastic morphology at confluence indicates COO^--SAMs are a favorable substrate for cell amplification. While confluent VIC cultures tend to undergo rapid conversion to obVICs,[8, 10, 40] COO^--SAMs do not exhibit such behavior, suggesting the negative charged environment plays a role in preventing osteoblastic differentiation of VICs.[18, 39, 43] Proliferation without confluent nodule formation supports the hypothesis for activation of VICs on negatively charged substrates similar to hyaluronic-acid rich valvulogenesis.[31] However, the lack of increased αSMA expression and protein (collagen or elastin),suggests secondary signaling may be required for healthy tissue production.

4.7. Cell-Material Phenotypic Signaling

It has been suggested that VICs in osteoblastic media do not become true osteoblasts due to a lack of osteoblastic expressed gene markers. This has led to the support of dystrophic calcification mechanisms in VICs.[52] In this study osteocalcin expression and an

osteoblastic morphology, suggest VIC phenotype on NH_3^+ SAMs may be more related to an osteogenic differentiation rather than dystrophic mechanisms. This is likely due to changes in integrin expression and focal adhesion formation resulting in up-regulation of an osteoblastic phenotype. Previous research has shown NH_3^+-SAMs expose more α5β1integrin binding domains, causing differentiation of pre-osteoblastic cell (MC3T3-E1) to osteoblasts.[39] Similar results using VICs and primary osteoblasts also indicate the necessity of α5β1 integrin binding in calcified nodule formation and osteoblastic gene expression.[18, 53]

Conversely, it has been observed that COO^- surfaces allow for greater binding availability of αvβ3, and reduced mineralization by MC3T3s, which was reversed when β3 binding was inhibited.[39] Furthermore, increased αvβ3 integrin expression in MC3T3s show increased proliferation but a down-regulation of osteocalcin and other osteoblastic markers similar to VICs on COO^--SAMs.[54] Although some correlations to integrins in research have been presented here, a more complete explanation of integrin expression and phenotype needs to be conducted to better understand the importance and influence of specific cell-material interactions on VIC phenotype. Once these are better understood a correlation between *in vitro* and *in vivo* conditions can be sought.

4.8. Experimental Limitations

It is well understood that self-assembled monolayers allow for the control of surface chemistry for investigating the effects on cell behavior. However, the use of gold-bound alkanethiolate SAMs on glass do present some experimental difficulties for comparison with *in vivo* tissue development, primarily though the use of stiff substrates [55] and two-dimensional environments. It has previously been observed that VIC growth on stiffer matrixes results in greater differentiation towards myofibroblastic and calcifying phenotypes.[6] However, this is also a limitation to standard methods of in vitro expansion of VICs on TCPS.

It is also well understood that variations in fetal bovine serum (FBS) can result in altered cell-behavior.[56] As batch-to-batch variations in FBS result in differences in protein constituents, the results of this work were collected utilizing a single lot of FBS to control growth environment. To accommodate for such changes, surfaces can be pre-incubated with specific proteins for creation of a more-homogeneous environment. However, even surfaces treated for single protein interactions can become attenuated upon addition of FBS as higher affinity proteins dissociate the adhered proteins before cell attachment.[38, 43, 57] As such when attempting to control cell-surface interactions it becomes important to characterize protein adlayers or utilize well-defined surfaces such as SAMs, which help to guide protein adsorption.[43, 58]

Furthermore, species-specific differences do exist between VICs in culture. These differences do lead to greater susceptibility of porcine VICs to develop calcified nodules in vitro. However, due to limited availability of human VICs and the tissue specific similarities between human and porcine heart tissue, porcine VICs remain the predominant cell type in literature used to investigate the development of valve stenosis.[59, 60]

5. Conclusions

Although VIC activation and proliferation can result in calcified nodule formation in confluent cultures, tissue mineralization is likely the result of several distinct mechanisms *in vitro*. Through variations in surface chemistry we have identified an osteoblastic-inhibiting environment (COO^-), and surfaces which possess characteristics of dystrophic calcification (CH_3) and osteogenic differentiation/calcification (NH_3^+). The rapid nodule formation by VICs on NH_3^+-SAMs may provide an accelerated *in vitro* model of heart valve disease, although additional studies remain to verify that our results resemble material mediated VIC differentiation in aortic valve disease *in vivo*. While cell-signaling cascades will be the subject of future investigations, these results establish surface-dependent effects on VIC phenotypic behavior. Using SAMs to study VIC behavior should also prove to be clinically relevant in guiding the selection of biomaterials for heart valve implants and tissue engineering scaffolds. Overall these results establish the importance of surface chemistry on VIC phenotypic behavior and establish SAMs as model surfaces for studying *in vitro* VIC differentiation.

Supplementary Material

Refer to Web version on PubMed Central for supplementary material.

Acknowledgments

We would like to thank Dr. Kateryna Artyushkova for assistance in X-ray photoelectron spectroscopy data acquisition and analysis, Dr. Linnea Ista for her assistance and expertise in alkanethiol self-assembled monolayers and manuscript editing, and David Santistevan for data formatting and manuscript editing.

Sources of Funding – This research was partially funded by the American Heart Association (10BGIA4570031) and NSF Career award (NSF CBET1351947). Educational support was provided by NSF IGERT (0504276), NSF LS-AMP (HER1026412 (BDVIII)), NIH IMSD (5R25-GM060201), and NIH PREP (R25GM075149) fellowships.

References

1. Go AS, Mozaffarian D, Roger VL, Benjamin EJ, Berry JD, Blaha MJ, Dai S, Ford ES, Fox CS, Franco S, Fullerton HJ, Gillespie C, Hailpern SM, Heit JA, Howard VJ, Huffman MD, Judd SE, Kissela BM, Kittner SJ, Lackland DT, Lichtman JH, Lisabeth LD, Mackey RH, Magid DJ, Marcus GM, Marelli A, Matchar DB, McGuire DK, Mohler ER 3rd, Moy CS, Mussolino ME, Neumar RW, Nichol G, Pandey DK, Paynter NP, Reeves MJ, Sorlie PD, Stein J, Towfighi A, Turan TN, Virani SS, Wong ND, Woo D, Turner MB. American Heart Association Statistics C, Stroke Statistics S. Heart disease and stroke statistics--2014 update: a report from the American Heart Association. Circulation. 2014; 129:e28–e292. [PubMed: 24352519]
2. Nkomo VT, Gardin JM, Skelton TN, Gottdiener JS, Scott CG, Enriquez-Sarano M. Burden of valvular heart diseases: a population-based study. Lancet. 2006; 368:1005–1011. [PubMed: 16980116]
3. Carabello BA, Crawford FA. Valvular heart disease. New Eng J Med. 1997; 337:32–41. [PubMed: 9203430]
4. Novaro GM, Griffin BP. Calcific aortic stenosis: Another face of atherosclerosis? Clev Clin J Med. 2003; 70:471–477.
5. Li C, Xu SY, Gotlieb AI. The progression of calcific aortic valve disease through injury, cell dysfunction, and disruptive biologic and physical force feedback loops. Cardiovasc Pathol. 2013; 22:1–8. [PubMed: 22795219]

6. Yip CYY, Chen JH, Zhao RG, Simmons CA. Calcification by valve interstitial cells Is regulated by the stiffness of the extracellular matrix. Arterioscler Thromb Vasc Bio. 2009; 29 936-U417.
7. Rajamannan NM, Evans FJ, Aikawa E, Grande-Allen KJ, Demer LL, Heistad DD, Simmons CA, Masters KS, Mathieu P, O'Brien KD, Schoen FJ, Towler DA, Yoganathan AP, Otto CM. Calcific aortic valve disease: not simply a degenerative process: A review and agenda for research from the National Heart and Lung and Blood Institute Aortic Stenosis Working Group. Executive summary: Calcific aortic valve disease-2011 update. Circulation. 2011; 124:1783–1791. [PubMed: 22007101]
8. Benton JA, Kern HB, Anseth KS. Substrate Properties Influence Calcification in Valvular Interstitial Cell Culture. J Heart Valve Dis. 2008; 17:689–699. [PubMed: 19137803]
9. Benton JA, Kern HB, Leinwand LA, Mariner PD, Anseth KS. Statins block calcific nodule formation of valvular interstitial cells by inhibiting alpha-smooth muscle actin expression. Arterioscler Thromb Vasc Biol. 2009; 29:1950–1957. [PubMed: 19679827]
10. Jian B, Narula N, Li QY, Mohler ER, Levy RJ. Progression of aortic valve stenosis: TGF-beta 1 is present in calcified aortic valve cusps and promotes aortic valve interstitial cell calcification via apoptosis. Ann Thorac Surg. 2003; 75:457–465. [PubMed: 12607654]
11. Clark-Greuel JN, Connolly JM, Sorichillo E, Narula NR, Rapoport HS, Mohler ER, Gorman JH, Gorman RC, Levy RJ. Transforming growth factor-beta 1 mechanisms in aortic valve calcification: Increased alkaline phosphatase and related events. Ann Thorac Surg. 2007; 83:946–953. [PubMed: 17307438]
12. Gould ST, Darling NJ, Anseth KS. Small peptide functionalized thiol-ene hydrogels as culture substrates for understanding valvular interstitial cell activation and de novo tissue deposition. Acta Biomater. 2012; 8:3201–3209. [PubMed: 22609448]
13. Duan B, Hockaday LA, Kapetanovic E, Kang KH, Butcher JT. Stiffness and adhesivity control aortic valve interstitial cell behavior within hyaluronic acid based hydrogels. Acta Biomater. 2013; 9:7640–7650. [PubMed: 23648571]
14. Mabry KM, Lawrence RL, Anseth KS. Dynamic stiffening of poly(ethylene glycol)-based hydrogels to direct valvular interstitial cell phenotype in a three-dimensional environment. Biomaterials. 2015; 49:47–56. [PubMed: 25725554]
15. Wang H, Haeger SM, Kloxin AM, Leinwand LA, Anseth KS. Redirecting Valvular Myofibroblasts into Dormant Fibroblasts through Light-mediated Reduction in Substrate Modulus. PLoS One. 2012; 7:12.
16. Duan B, Kapetanovic E, Hockaday LA, Butcher JT. Three-dimensional printed trileaflet valve conduits using biological hydrogels and human valve interstitial cells. Acta Biomater. 2014; 10:1836–1846. [PubMed: 24334142]
17. Gu XX, Masters KS. Role of the MAPK/ERK pathway in valvular interstitial cell calcification. Am J Physiol-Heart Circul Physiol. 2009; 296:H1748–H1757.
18. Gu XX, Masters KS. Regulation of valvular interstitial cell calcification by adhesive peptide sequences. J Biomed Mater Res Part A. 2010; 93A:1620–1630.
19. Rodriguez KJ, Masters KS. Regulation of valvular interstitial cell calcification by components of the extracellular matrix. J Biomed Mater Res Part A. 2009; 90A:1043–1053.
20. Gwanmesia P, Ziegler H, Eurich R, Barth M, Kamiya H, Karck M, Lichtenberg A, Akhyari P. Opposite Effects of Transforming Growth Factor-beta 1 and Vascular Endothelial Growth Factor on the Degeneration of Aortic Valvular Interstitial Cell Are Modified by the Extracellular Matrix Protein Fibronectin: Implications for Heart Valve Engineering. Tissue Eng Part A. 2010; 16:3737–3746. [PubMed: 20673026]
21. Rodriguez KJ, Piechura LM, Porras AM, Masters KS. Manipulation of valve composition to elucidate the role of collagen in aortic valve calcification. BMC Cardiovasc Disord. 2014; 14:10. [PubMed: 24461008]
22. Liu AC, Joag VR, Gotlieb AI. The emerging role of valve interstitial cell phenotypes in regulating heart valve pathobiology. Am J Pathol. 2007; 171:1407–1418. [PubMed: 17823281]
23. Hutcheson J, Chen J, Sewell-Loftin M, Ryzhova L, Fisher C, Su Y, Merryman W. Cadherin-11 Regulates Cell-Cell Tension Necessary for Calcific Nodule Formation by Valvular Myofibroblasts. Arterioscler Thromb Vasc Biol. 2013; 33:114–121. [PubMed: 23162011]

24. Desmouliere A, Badid C, BochatonPiallat ML, Gabbiani G. Apoptosis during wound healing, fibrocontractive diseases and vascular wall injury. Int J Biochem Cell Biol. 1997; 29:19–30. [PubMed: 9076938]
25. Mohler ER, Gannon F, Reynolds C, Zimmerman R, Keane MG, Kaplan FS. Bone formation and inflammation in cardiac valves. Circulation. 2001; 103:1522–1528. [PubMed: 11257079]
26. Wirrig EE, Hinton RB, Yutzey KE. Differential expression of cartilage and bone-related proteins in pediatric and adult diseased aortic valves. J Mol Cell Cardiol. 2011; 50:561–569. [PubMed: 21163264]
27. Merryman WD, Schoen FJ. Mechanisms of Calcification in Aortic Valve Disease: Role of Mechanokinetics and Mechanodynamics. Curr Cardiol Rep. 2013; 15:7.
28. Rajamannan NM, Subramaniam M, Rickard D, Stock SR, Donovan J, Springett M, Orszulak T, Fullerton DA, Tajik AJ, Bonow RO, Spelsberg T. Human aortic valve calcification is associated with an osteoblast phenotype. Circulation. 2003; 107:2181–2184. [PubMed: 12719282]
29. Schoen FJ, Levy RJ. Calcification of tissue heart valve substitutes: Progress toward understanding and prevention. Ann Thorac Surg. 2005; 79:1072–1080. [PubMed: 15734452]
30. Bain CD, Troughton EB, Tao YT, Evall J, Whitesides GM, Nuzzo RG. Formation of monolayer films by the spontaneous assembly of organic thiols from solution onto gold. J Am Chem Soc. 1989; 111:321–335.
31. Butcher JT, Markwald RR. Valvulogenesis: the moving target. Philos Trans R Soc Lond B Biol Sci. 2007; 362:1489–1503. [PubMed: 17569640]
32. Schroeder JA, Jackson LF, Lee DC, Camenisch TD. Form and function of developing heart valves: coordination by extracellular matrix and growth factor signaling. J Mol Med. 2003; 81:392–403. [PubMed: 12827270]
33. Khan MMT, Ista LK, Lopez GP, Schuler AJ. Experimental and theoretical examination of surface energy and adhesion of nitrifying and heterotrophic bacteria using self-assembled monolayers. Environ Sci Technol. 2011; 45:1055–1060. [PubMed: 21189005]
34. Creager SE, Clarke J. Contact-angle titrations of mixed omega-mercaptoalkaonic acid alkanethio monolayers on gold-reactive vs nonreactive spreading, and chain length effects of surface pKa values. Langmuir. 1994; 10:3675–3683.
35. Fears KP, Creager SE, Latour RA. Determination of the surface pK of carboxylic-and amine-terminated alkanethiols using surface plasmon resonance spectroscopy. Langmuir. 2008; 24:837–843. [PubMed: 18181651]
36. Faucheux N, Schweiss R, Lutzow K, Werner C, Groth T. Self-assembled monolayers with different terminating groups as model substrates for cell adhesion studies. Biomaterials. 2004; 25:2721–2730. [PubMed: 14962551]
37. Keselowsky BG, Collard DM, Garcia AJ. Surface chemistry modulates fibronectin conformation and directs integrin binding and specificity to control cell adhesion. J Biomed Mater Res A. 2003; 66:247–259. [PubMed: 12888994]
38. Arima Y, Iwata H. Effect of wettability and surface functional groups on protein adsorption and cell adhesion using well-defined mixed self-assembled monolayers. Biomaterials. 2007; 28:3074–3082. [PubMed: 17428532]
39. Keselowsky BG, Collard DM, Garcia AJ. Integrin binding specificity regulates biomaterial surface chemistry effects on cell differentiation. Proc Natl Acad Sci USA. 2005; 102:5953–5957. [PubMed: 15827122]
40. Mohler ER, Chawla MK, Chang AW, Vyavahare N, Levy RJ, Graham L, Gannon FH. Identification and characterization of calcifying valve cells from human and canine aortic valves. J Heart Valve Dis. 1999; 8:254–260. [PubMed: 10399657]
41. Blevins TL, Carroll JL, Raza AM, Grande-Allen KJ. Phenotypic Characterization of Isolated Valvular Intersitial Cell Subpopulations. J Heart Valve Dis. 2006; 15:815–822. [PubMed: 17152790]
42. Mrksich M. Using self-assembled monolayers to model the extracellular matrix. Acta Biomater. 2009; 5:832–841. [PubMed: 19249721]

43. Lin JH, Chang HY, Kao WL, Lin KY, Liao HY, You YW, Kuo YT, Kuo DY, Chu KJ, Chu YH, Shyue JJ. Effect of Surface Potential on Extracellular Matrix Protein Adsorption. Langmuir. 2014; 30:10328–10335. [PubMed: 25111830]
44. Mrksich M, Whitesides GM. Using self-assembled monolayers to understand the interactions of man-made surfaces with proteins and cells. Annu Rev Biophys Biomolec Struct. 1996; 25:55–78.
45. Lan MA, Gersbach CA, Michael KE, Keselowsky BG, Garcia AJ. Myoblast proliferation and differentiation on fibronectin-coated self assembled monolayers presenting different surface chemistries. Biomaterials. 2005; 26:4523–4531. [PubMed: 15722121]
46. Latif N, Sarathchandra P, Taylor PM, Antoniw J, Brand N, Yacoub MH. Characterization of molecules mediating cell-cell communication in human cardiac valve interstitial cells. Cell Biochem Biophys. 2006; 45:255–264. [PubMed: 16845172]
47. Xia H, Nho RS, Kahm J, Kleidon J, Henke CA. Focal adhesion kinase is upstream of phosphatidylinositol 3-kinase/Akt in regulating fibroblast survival in response to contraction of type I collagen matrices via a beta(1) integrin viability signaling pathway. J Biol Chem. 2004; 279:33024–33034. [PubMed: 15166238]
48. Chen J, Peacock JR, Branch J, Merryman WD. Biophysical Analysis of Dystrophic and Osteogenic Models of Valvular Calcification. J Biomech Eng-Trans ASME. 2015; 137:6.
49. Kielty CM, Sherratt MJ, Shuttleworth CA. Elastic fibres. J Cell Sci. 2002; 115:2817–2828. [PubMed: 12082143]
50. Sabatier L, Chen DL, Fagotto-Kaufmann C, Hubmacher D, McKee MD, Annis DS, Mosher DF, Reinhardt DP. Fibrillin Assembly Requires Fibronectin. Mol Biol Cell. 2009; 20:846–858. [PubMed: 19037100]
51. Silin V, Weetall H, Vanderah DJ. SPR studies of the nonspecific adsorption kinetics of human IgG and BSA on gold surfaces modified by self-assembled monolayers (SAMs). J Colloid Interface Sci. 1997; 185:94–103. [PubMed: 9056309]
52. Monzack EL, Masters KS. Can Valvular Interstitial Cells Become True Osteoblasts? A Side-by-Side Comparison. J Heart Valve Dis. 2011; 20:449–461. [PubMed: 21863660]
53. Moursi AM, Globus RK, Damsky CH. Interactions between integrin receptors and fibronectin are required for calvarial osteoblast differentiation in vitro. J Cell Sci. 1997; 110:2187–2196. [PubMed: 9378768]
54. Cheng SL, Lai CF, Blystone SD, Avioli LV. Bone mineralization and osteoblast differentiation are negatively modulated by integrin alpha v beta 3. J Bone Miner Res. 2001; 16:277–288. [PubMed: 11204428]
55. DelRio FW, Jaye C, Fischer DA, Cook RF. Elastic and adhesive properties of alkanethiol self-assembled monolayers on gold. Appl Phys Lett. 2009; 94:3.
56. Zheng XY, Baker H, Hancock WS, Fawaz F, McCaman M, Pungor E. Proteomic analysis for the assessment of different lots of fetal bovine serum as a raw material for cell culture. Part IV. Application of proteomics to the manufacture of biological drugs. Biotechnol Prog. 2006; 22:1294–1300. [PubMed: 17022666]
57. Thomas CH, McFarland CD, Jenkins ML, Rezania A, Steele JG, Healy KE. The role of vitronectin in the attachment and spatial distribution of bone-derived cells on materials with patterned surface chemistry. J Biomed Mater Res. 1997; 37:81–93. [PubMed: 9335352]
58. Liu LY, Chen SF, Giachelli CM, Ratner BD, Jiang SY. Controlling osteopontin orientation on surfaces to modulate endothelial cell adhesion. J Biomed Mater Res Part A. 2005; 74A:23–31.
59. Bowler MA, Merryman WD. In vitro models of aortic valve calcification: solidifying a system. Cardiovasc Pathol. 2015; 24:1–10. [PubMed: 25249188]
60. Cloyd KL, El-Hamamsy I, Boonrungsiman S, Hedegaard M, Gentleman E, Sarathchandra P, Colazzo F, Gentleman MM, Yacoub MH, Chester AH, Stevens MM. Characterization of Porcine Aortic Valvular Interstitial Cell 'Calcified' Nodules. PLoS One. 2012; 7:9.

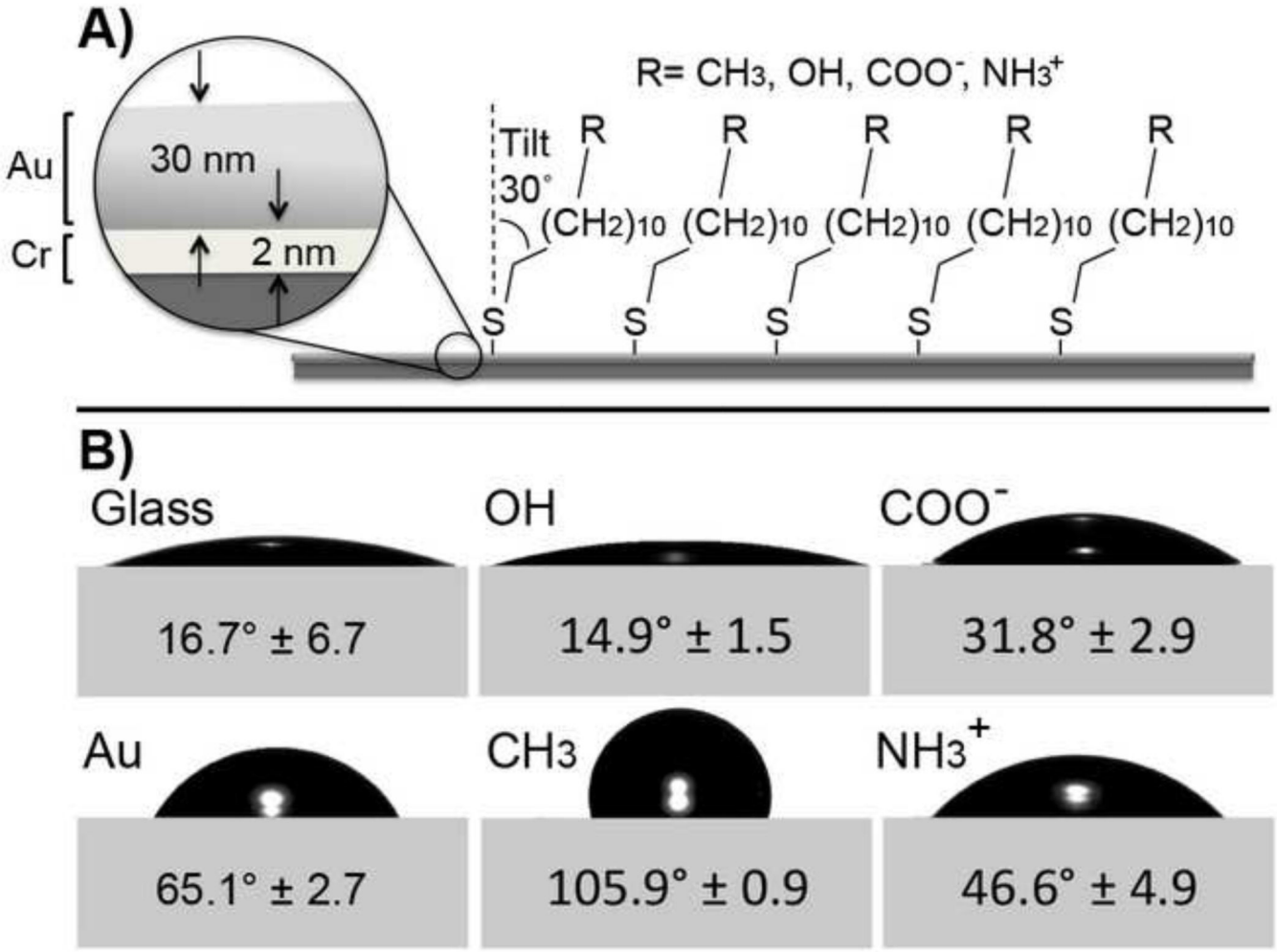

Figure 1.

A) Schematic of alkanethiol self-assembled monolayer (SAM) on gold (Au, 30nm) coated glass with chromium (Cr, 2nm) adhesion layer. B) Air-water-surface contact angles determined using the sessile drop goniometry (ultrapure H_2O in air).

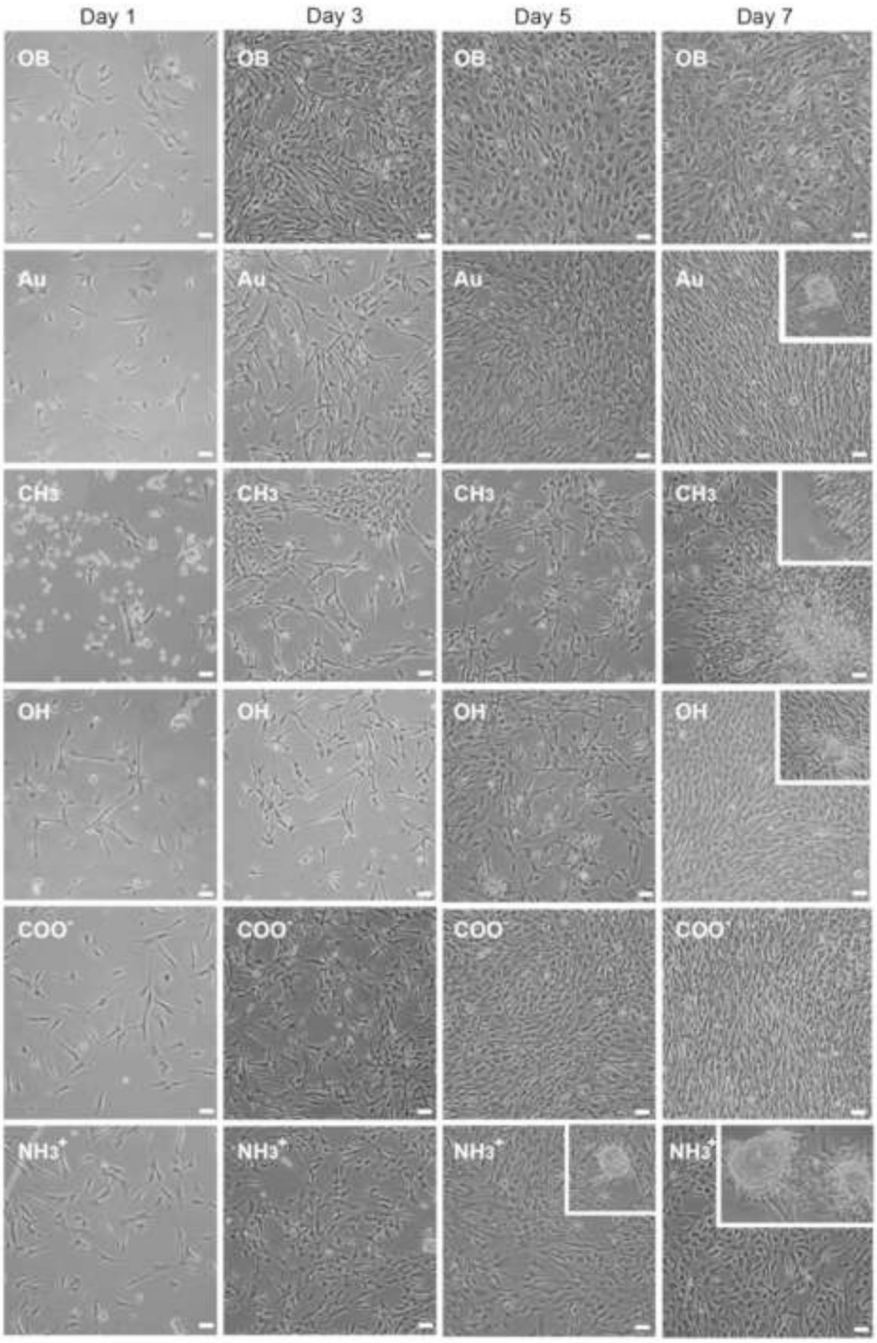

Figure 2.

Valvular interstitial cell (VIC) proliferation on monolayer surfaces as compared to bare glass/osteoblastic (OB) and gold controls (dashed lines). Initial inhibition of VIC growth (1–3 days) is exhibited by OH and CH_3-SAMs with significant lower cell concentration, while osteoblastic (OB) controls are significantly greater than other treatments. Between 3 and 5 days, VICs on OH-SAMs begin proliferation while CH_3-SAMs result in significantly lower cell concentration throughout the experiment. By day 5, COO^--SAMs have significantly

higher cell concentrations than any other treatment. Between five and seven days in culture all samples, except CH_3-SAMs, reach confluence. *$p < 0.05$, $n = 6$.

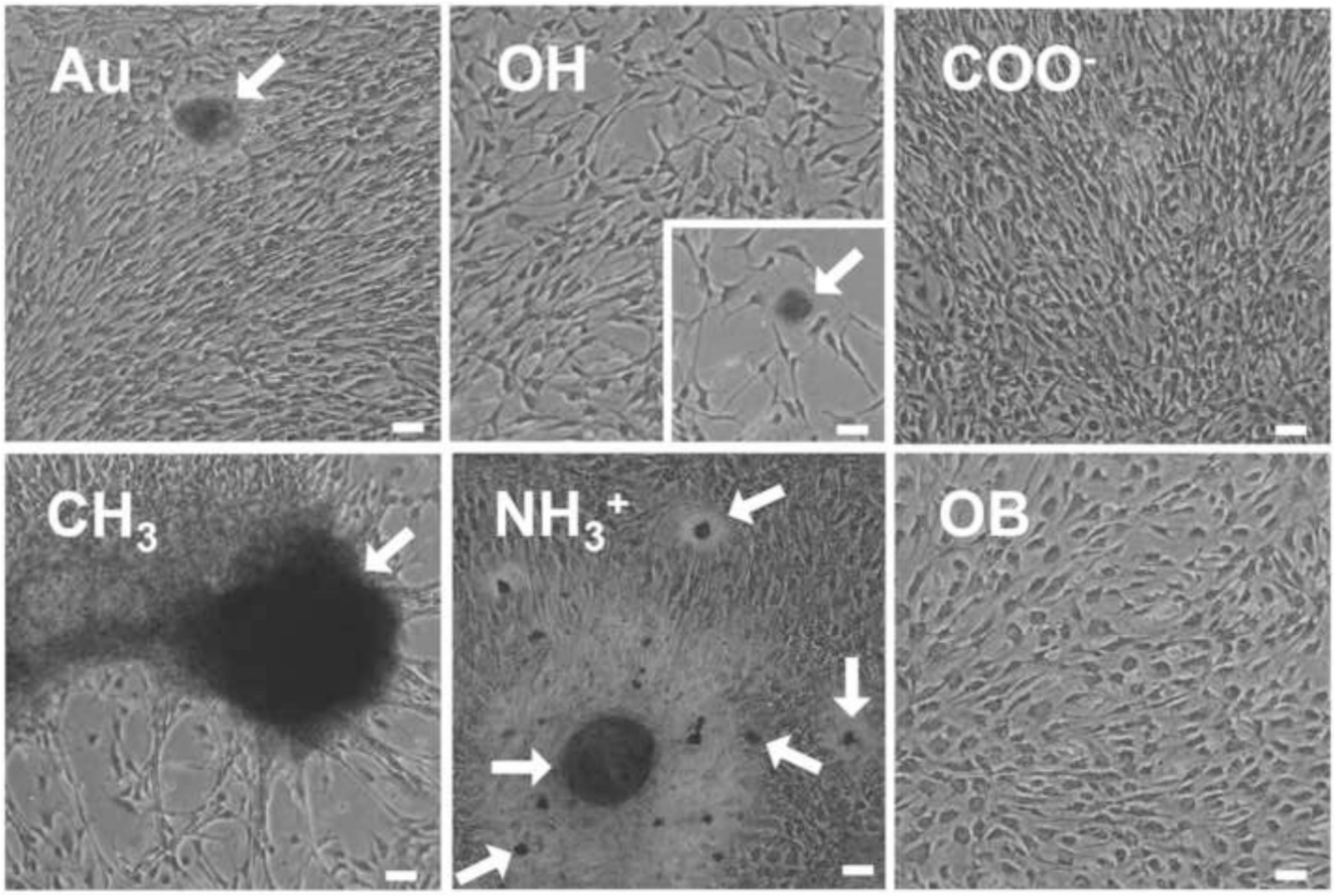

Figure 3.

Bright field (phase contrast) representative images of cell morphology on varying surfaces chemistry compared to gold (Au) and osteoblastic controls over seven days of growth. Day 5 and 7, insets show morphology and relative size of nodules formed in culture, COO^{-} surfaces did not show any nodule formation over the course of this study. Further images can be found in online data supplement. Scale = 50 μm, inset images same scale.

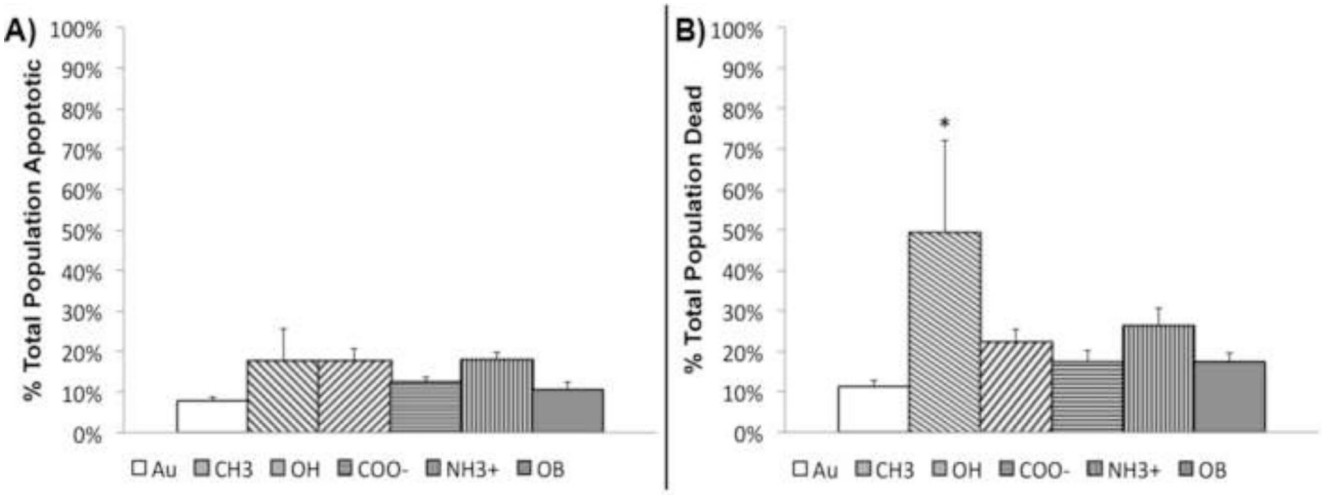

Figure 4.

Representative images of alizarin red S calcium staining after seven days of growth. Arrows indicate distinct calcium-stained nodules. Scale = 50μm

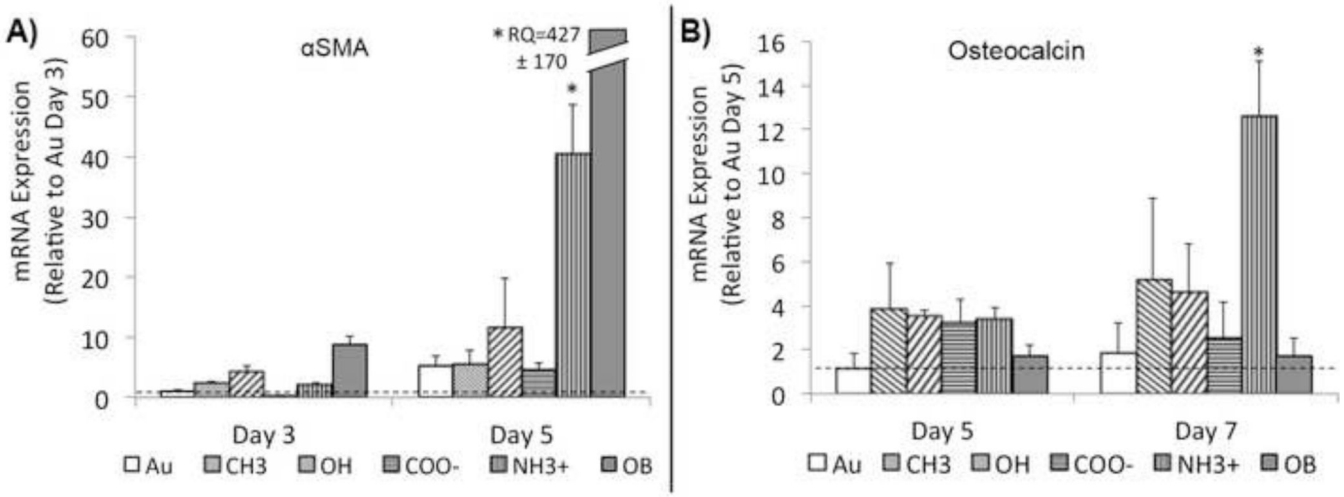

Figure 5.

Measurement of valvular interstitial cell A) apoptosis and B) overall cell death after seven days. CH_3-SAMs result in significant increase of dead cells over all other treatments. Cell death assessed through measurement of annexin V activity (apoptosis) and propidium iodide infiltration (dead). *$p < 0.05$, $n = 6$.

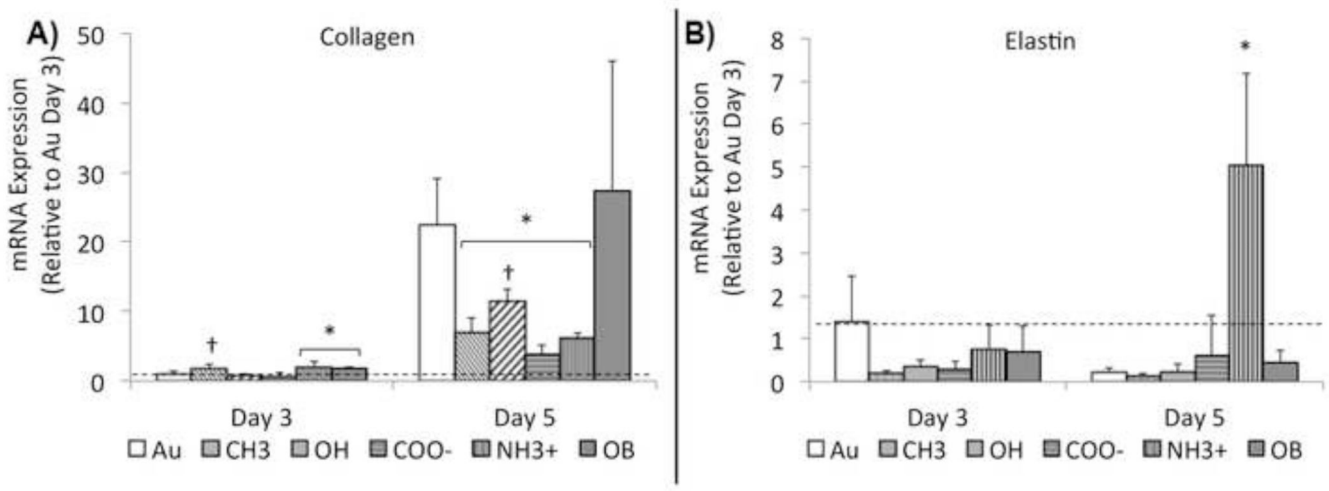

Figure 6.

A) α-smooth muscle actin (αSMA) and B) osteocalcin (OCN) geneexpression (mRNA) by valvular interstitial cells (VICs) at later stages of growth on functionalized surfaces. Initial expression of αSMA visualized through immunocytochemical staining (data not shown) is reduced by day 5 on most surfaces except NH_3^+-SAMs and osteoblastic controls, which have a significantly higher in αSMA expression. NH_3^+-SAMs also express significant increases in OCN expression (a late stage osteoblastic marker observed in between days 14 & 21 in osteoblast-like VICs) as early as day 7. *$p < 0.05$, $n = 6$.

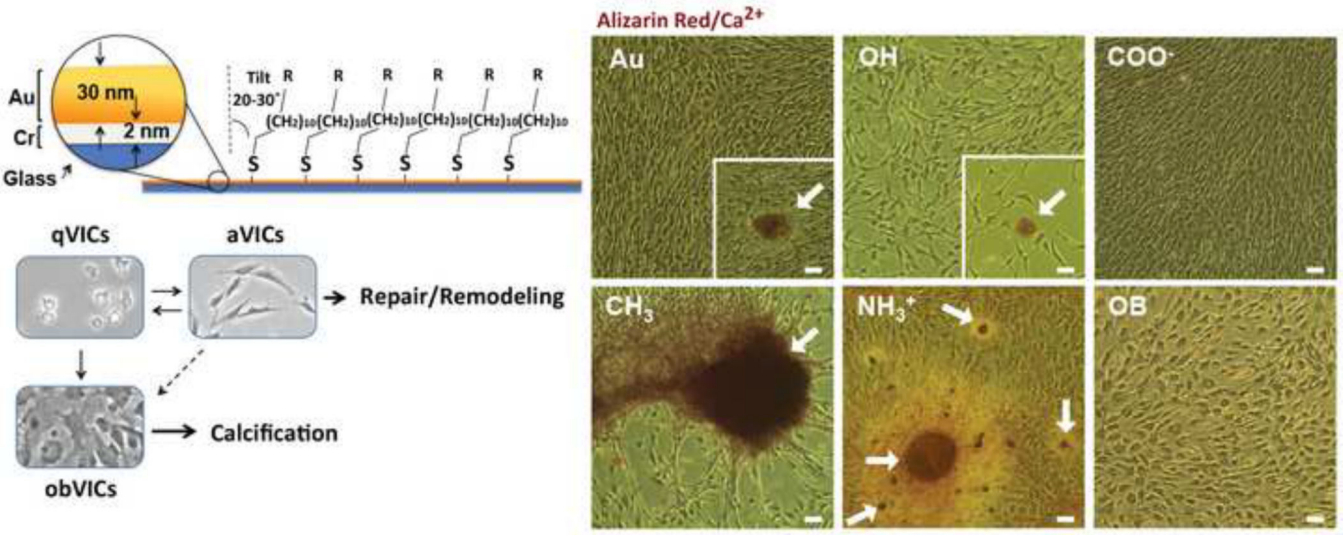

Figure 7.

A) Collagen-I and B) Elastin genetic expression (mRNA) by valvular interstitial cells (VICs) at three and five days of growth on functionalized surfaces. After 3 days, collagen is up regulated on NH_3^+-SAMs and media induced osteoblastic controls. Elevated collagen expression was also observed on CH_3-SAMs, but results were not statistically different from Au controls. Collagen expression is significantly greater in all treatments between days 3 and 5. By day 5, all SAMs treatments are significantly lower than Au controls. * Indicates a statistically significant difference ($p < 0.05$) between treatments and Au controls and † indicates significant differences among SAMs treatments, $n = 4$.

Table 1

Calcified tissue/nodule diameter after 7 days.

Treatment	Average Nodule Diameter (μm)
Au	60.5 ± 27.0
CH_3 †	221 ± 123*
OH	29.8 ± 10.9
COO^-	-
NH_3^+ ‡	115 ± 39.8*
OB	-

(−) No nodules observed during culture

† Highly irregular cellular aggregates, no distinct boundary

‡ Tightly bound, spherical calcium nodules